The 44th William Blum Lecture
Presented at the 90th AESF Annual Convention (SUR/FIN 2003)
in Nashville, Tennessee
June 24, 2003

Electrodeposition of Alloys and Composites with Superior Corrosion and Electrocatalytic Properties

by
Prof. Branko N. Popov
Recipient of the 2002 William Blum
Scientific Achievement Award

The 44th William Blum Lecture
Presented at the 90th AESF Annual Convention (SUR/FIN 2003)
in Nashville, Tennessee
June 24, 2003

Electrodeposition of Alloys and Composites with Superior Corrosion and Electrocatalytic Properties

by
Prof. Branko N. Popov
Recipient of the 2002 William Blum
Scientific Achievement Award

Originally published as
Plating & Surface Finishing, 91 (10), 40-49 (2004)

Editor's Note: This article is a re-publication of the 44th William Blum Lecture, presented at the 90th AESF Annual Convention (SUR/FIN 2003) in Nashville, Tennessee on June 24, 2003.

ABSTRACT

Tremendous potential exists for the growth of the metal finishing industry in this century through the development of processes that are either environmentally friendly or are applicable at the nanoscale. The chemical composition and the structure of electrodeposited metals, alloys and composites control their functional properties. This paper will discuss some of the theoretical and experimental studies done to achieve such coatings. Nanostructured alloys and innovative composite materials were developed through adaptation of existing bath chemistries. Process development was based on techniques developed in our laboratories such as: under potential deposition (UPD) of monoatomic metal layers, autocatalytic reduction and potentiostatic pulse (PP) plating of layers of amorphous and crystalline nanostructured metals and alloys. The development processes have been optimized based on obtaining superior corrosion and electrocatalytic properties. Further refinement of the coating process was achieved through the development of first principles based theoretical models.

Electrodeposited nanostructured alloys and composites find applications in metals and the surface finishing industry. This paper will feature the development of electrochemical deposition processes to synthesize secondary and ternary alloys such as Ni-Zn-X (X=P or Cd). These materials were targeted as a replacement for Cd deposition and can inhibit corrosion and completely eliminate the hydrogen induced cracking.

Electrodeposited nanostructured metals and alloys are also applicable in electronics and in the next generation of batteries, supercapacitors and fuel cell assemblies. With increasing miniaturization of electronic devices, current focus is on developing portable energy sources that can power these devices. The paper will demonstrate that pulse electrodeposition is an attractive method for controlling composite microstructure and morphology, thus yielding superior electrocatalytic properties.

Current research and challenges

The practical use of steel and high strength alloys is limited by corrosion and cracking hazards due to hydrogen penetration and hydrogen accumulation in the bulk of these alloys.[1-4] According to our earlier studies,[5-15] polarization and permeation experiments showed that electrodeposited lead and bismuth nanostructured layers inhibited the evolution and penetration of hydrogen through AISI 4340 steel alloy and Inconel 718 alloy. The corrosion rate and hydrogen permeation[16] were also inhibited in the presence of underpotentially deposited (UPD) zinc.[7] Hydrogen evolution exchange current density, surface coverage, absorption-adsorption reaction constant and the hydrogen recombination constant were estimated on bare iron and zinc plated iron.[14,17] The observed effects were due to kinetic limitations of the hydrogen discharge reaction and suppression of the hydrogen absorption by the deposited monolayers.

Nanostructured multiple zinc layers with superior corrosion properties were deposited on iron using a solution containing 1.0M H_3BO_3, 1.0M Na_2SO_4, 0.4M NaCl with the addition of 0.05M $ZnSO_4$.[18] Electroplated nanostructured multiple zinc layers inhibited the corrosion rate and the permeation current an average of 93 and 96%, respectively, as compared with bare iron. However, due to a large difference in electronegativity between iron and zinc, the zinc corrosion rate is still higher when compared to cadmium plates.[19]

A cadmium electroplate on steel has many advantages such as good lubricity, solderability and low galvanic corrosion with aluminum.[19,20] Cadmium plating offers an effective barrier protection to the substrate, especially in the marine environment. Apart from this, cadmium also offers sacrificial protection[21] to the steel components under corroding conditions. However, cadmium deposition from cyanide baths gives rise to unacceptably high hydrogen intake[22] by plated components of high strength, leading to hydrogen embrittlement. Also cyanide waste treatment[23] is very expensive. Thus, environmental concerns and performance criteria mandate the research need for alternatives to cadmium coatings. Efforts have been made worldwide to develop alternate, non-cyanide baths for cadmium plating, based on sulfamate, flouborate and chloride.[24,25] However, these baths have not been satisfactory.[26] To increase the barrier properties of zinc coating, research has been aimed at developing effective zinc based coating by alloying zinc with a more noble metal such as nickel.

The current technology available for Zn-Ni plating includes both alkaline and acid plating.[27-29] Deposit characteristics of Zn-Ni as compared to the conventional zinc include benefits of extended corrosion resistance and significantly harder deposits. Also, the presence of nickel imparts a good barrier resistance to the coating. Several studies have been done previously to optimize the composition of Zn-Ni alloys based on corrosion performance analysis.[30-35] Baldwin and his co workers showed[30-31] that an optimum level of corrosion protection was obtained in case of alloys containing approximately 14 wt% of nickel. Zinc alloy electrodeposits formed with other metals such as cobalt[34-37], iron[38], tin[39] and manganese[40-41] are also of interest. Some of the zinc based alloys have better or equal corrosion resistance to that of cadmium deposits.[42] However, due to the high zinc content in the deposit, these alloys are more negative than cadmium and hence dissolve rapidly in any corrosive environments. The mechanism for this preferential deposition has been discussed extensively in literature.[43-44] Typical nickel composition in the Zn-Ni alloy is approximately 10-15%, and any further increase in nickel composition is based on using a higher-than-predicted Ni/Zn ratio in the bath.[29,45]

Attempts were made to decrease the anomaly in the case of Zn-Ni alloys and increase the nickel content by either introducing inert species in the bath or by developing a ternary alloy.[46-54] Slower kinetics rather than concentration overpotential compensate for the potential drop, which occurs in the presence of nonyl phenyl polyethylene oxide (NPPO). Studies have also been done to include inert materials such as SiO_2 in the deposit.[55-56] Such deposits possess superior corrosion properties compared to the bare alloy. Zhou, *et. al.*[50] have studied the effect of tin additions on the anomalous deposition of Zn-Ni alloy. The nickel ratio increased from 6 to 8% with the addition of small amounts of tin. However, the observed small increase of Ni content in the alloy didn't improve the Zn-Ni barrier properties.

In summary, an enhancement in the nickel composition would lead to more anodic open circuit potential, which in turn will reduce the driving force for the galvanic corrosion. Also, the barrier properties associated with nickel rich deposits are superior compared to other coatings.

The approach taken in our work was to develop the electroless or electrodeposition process for plating Zn-Ni-X (X=P, Cd) alloys, which will induce barrier properties to the sacrificial Zn-Ni alloy. By introducing a new element in the Zn-Ni alloy one can expect to decrease the Zn-Ni ratio in the alloy and consequently, to decrease the Zn-Ni alloy corrosion potential from -1.14 V_{SCE}, to even lower values than the corrosion potential of Cd (-0.79 V_{SCE}). Also by introducing a third element in the alloy, the goal was to modify the rate of the hydrogen evolution reaction, the hydrogen proton recombination and adsorption kinetics at the surface in order to inhibit corrosion and completely impede hydrogen penetration in the alloy, thus eliminating the hydrogen embrittlement.

Development of amorphous Ni-Zn-P alloy coatings

Autocatalytic reduction offers an attractive method to obtain deposits with high Ni content (85-90%).[57-59] Since the zinc content in the alloy is lower than 10%, the alloy corrosion potential is
-0.476 V_{SCE}, which is more positive than the corrosion potential of steel, -0.590 V_{SCE}. Thus, these deposits cannot be used as a sacrificial coating for steel. A theoretical kinetic model based on mixed potential theory[60-61] was developed to explain the

processes occurring during the electroless deposition of the Ni-Zn-P alloy from alkaline electrolytes with the objectives of enhancing the zinc content in the alloy and ensuring that the coating will exhibit sacrificial properties. The model simulates the surface coverage of Zn, Ni and P under various bath conditions. Rotating disc electrode (RDE) studies and surface characterization techniques have been used extensively to understand the Ni-Zn-P electroless process. The model simulations were compared to the experimental data obtained using RDE experiments.[60]

To optimize the alloy composition, plating and subsequent corrosion studies were carried out on low carbon cold-rolled steel foils of thickness 0.5 mm and area 25 x 25 mm. Ni-Zn-P composites were prepared from a bath containing 35 g/L $NiSO_4$, complexing agents and 50 g/L NH_4Cl. Sodium hypophosphite was used as a reducing agent for the autocatalytic process and as a source of phosphorus in the final deposit. The pH was maintained at 10.5 during the deposition.[61]

Our initial studies indicated that zinc cannot be deposited autocatalytically in the absence of nickel ions from the electrolyte given above. The measured mixed potential in the same electrolyte was found to depend upon the concentration of zinc ions in the bath and varied between -1.071 V_{SCE} (5 g/L $ZnSO_4$) and -1.036 V_{SCE} (20 g/L $ZnSO_4$). On the other site, it was possible to deposit Zn-Ni alloy at -1.036 V_{SCE} electrochemically or by using an electroless technique when nickel ions were present in the electrolyte, indicating that the nickel catalyzes the zinc deposition at this potential. The cathodic and anodic reactions of any of the autocatalytic processes are independent when they occur simultaneously.[61] Thus, it is possible to study the anodic polarization of hypophosphate in the presence and absence of ions on different catalytic surfaces because it would represent the true anodic current that would occur in the complete bath. To determine why zinc will deposit in the presence of nickel ions, the hypophosphate oxidation was carried out on a nickel substrate in the presence of only complexing agents. The hypophosphate oxidation curve obtained on nickel is shown in Fig. 1.

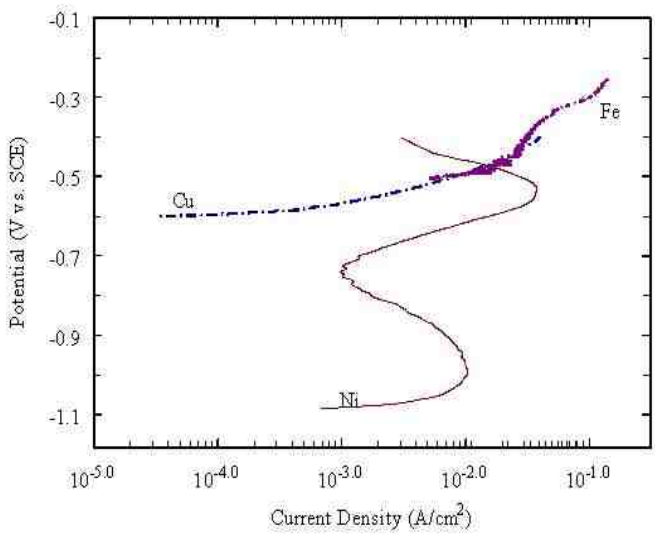

Figure 1 - Polarization studies of hypophosphite oxidation on different substrates.

As shown, the nickel surface catalyzes the hypophosphate oxidation reaction, since an anodic current attributable to the oxidation of hypophosphate was not observed on copper or iron. Thus, in the case of electroless deposition of Zn-Ni alloys, the reaction is initiated by a spontaneous displacement reaction between the iron substrate and the nickel ions present at the interface. As a result, iron dissolves while nickel deposits on the surface. The thin nickel film thus formed causes the oxidation of hypophosphate to occur at potentials higher than -1.0 V_{SCE}, which enables zinc reduction and formation of Ni-Zn-P alloy.

The pH of the bath plays a very important role in determining the composition of the Ni-Zn deposits. A complete analysis of the equilibrium reactions between various species was performed to analyze the effect of pH on the concentration of the electroactive species in the bath. According to the Pourbaix pH–potential diagrams of zinc and nickel, both metals precipitate to form their respective hydroxides with an increase of pH above 7.00. The presence of a complexing agent such as ammonia prevents the precipitation. In the presence of ammonia, the following complexes are formed:

$$Zn^{+2} + 2OH^- \rightarrow Zn(OH)_2 \quad (1)$$

$$Ni^{+2} + 2OH^- \rightarrow Ni(OH)_2 \quad (2)$$

$$Ni(OH)_2 + 6NH_3 \rightarrow Ni(NH_3)_6^{+2} + 2OH^- \quad (3)$$

Zn and nickel complexes reduce to deposit a Zn-Ni alloy with the liberation of ammonia.

$Zn(NH_3)_4^{+2} + 2e^- \rightarrow Zn + 4NH_3$ (4)

$Ni(NH_3)_4^{+2} + 2e^- \rightarrow Ni + 6NH_3$ (5)

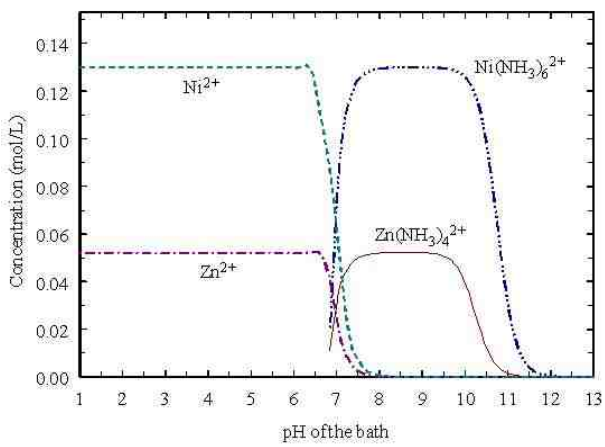

Figure 2 - Variation in equilibrium concentrations of complexed Zn and Ni species as a function of bath pH.

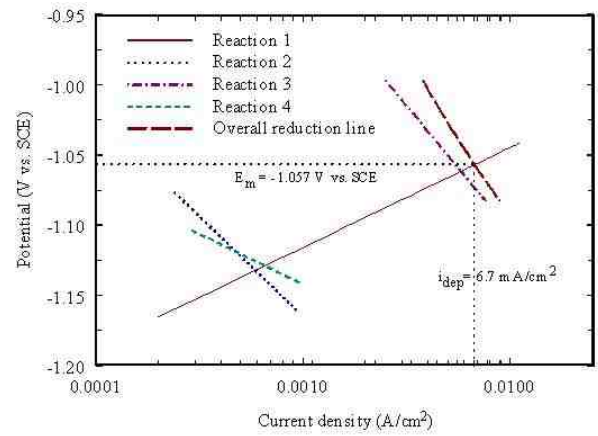

Figure 3 - Evans diagram showing the various reactions happening during the electroless depo-sition process for a $ZnSO_4$ concentration of 5 g/L.

Material balances coupled with various equilibrium relations and electroneutrality conditions were used to plot the pH – concentration diagram. Figure 2 shows the equilibrium concentration of different electroactive species as a function of bath pH. The concentration of the zinc and nickel complexes varies with an increase of pH above 9.0. The concentration ratio of the nickel complex to the zinc complex increases with an increase in pH. This variation in the concentration of nickel and zinc complexes is expected to favor the nickel deposition from alkaline electrolytes.

Figure 3 shows the Evans diagram for the processes occurring at the electrode-electrolyte interface during the Zn-Ni-P autocatalytic deposition. The system was simulated for a $ZnSO_4$ concentration of 5 g/L. The following reactions were considered: [63,64]

$H_2PO_2^- + H_2O$ —Catalytic Surface→ $H_2PO_3^- + 2H^+ + 2e^-$ (6)

$2H_2PO_2^- + H^+ + e^- \rightarrow P + HPO_3^{-2} + H_2O + H_2\uparrow$ (7)

$Ni(NH_3)_6^{+2} + 2e^- \rightarrow Ni + 6NH_3$ (8)

$Zn(NH_3)_4^{+2} + 2e^- \rightarrow Zn + 4NH_3$ (9)

$2H^+ + 2e^- \rightarrow H_2\uparrow$ (10)

The equilibrium potential for each reaction is given by

$$E_{eq,j} = E_{0,j} + \frac{2.303RT}{n_j F}\log\frac{\prod c_{oxi}}{\prod c_{red}} \qquad (11)$$

where E_o is the standard potential for each reaction. For simplicity, the activity of $H_2PO_3^-$ and HPO_3^{-2} is assumed to be unity for determining the equilibrium potentials of reactions 6 and 7. In the case of Zn and Ni, the equilibrium potentials was estimated using the following relation:

$$E_{eq,j} = E_{0,j} + \frac{2.303RT}{n_j F}\log K_j + \frac{2.303RT}{n_j F}\log\frac{\prod c_{oxi}}{\prod c_{red}} \tag{12}$$

where K_j is the stability constant of the complexed species. The intercepts for all partial reactions were calculated based on the effective exchange current density, given by the product of the equilibrium exchange current density and the surface coverage of the species involved in the reaction.[60] Assuming Tafel approximations, the current density for the anodic reaction is given by

$$i_1 = i_{0,1}(\theta_{H_2PO_2})^{0.5}(\theta_H)\exp\left[\frac{(1-\beta_1)n_1F}{RT}\eta_1\right] \tag{13}$$

while the cathodic current densities are:

$$|i_2| = i_{0,2}\left(\theta_{H_2PO_2}\right)\left(\theta_H\right)^{0.5}\exp(-\frac{\beta_2 n_2 F}{RT}\eta_2) \tag{14}$$

$$|i_3| = i_{0,3}\left(\theta_{Ni}\right)^{0.8}\exp(-\frac{\beta_3 n_3 F}{RT}\eta_3) \tag{15}$$

$$|i_4| = i_{0,4}\left(\theta_{Zn}\right)^{0.5}\exp(-\frac{\beta_4 n_4 F}{RT}\eta_4) \tag{16}$$

$$|i_5| = i_{0,5}\left(\theta_H\right)^{0.6}\exp(-\frac{\beta_5 n_5 F}{RT}\eta_5) \tag{17}$$

where η_j is the overpotential and β_j is the symmetry factor for the respective reactions. Thus the total oxidation current is the sum of all of the above partial currents.

The surface coverage for each species follows an equilibrium isotherm of the form:

$$\theta_j = \frac{b_j C_{s,j}}{1 + b_j C_{s,j}} \tag{18}$$

where b_j is the concentration dependent adsorption coefficient for each of the reacting species. As shown in Figure 3, the partial current density for Ni deposition is much higher than those observed for Zn and P deposition. The potential at which the oxidation line and the overall reduction line crosses is the mixed potential of the deposition process. The current density at the intersection corresponds to the electroless plating current density.

Figure 4 compares the model and experimental mixed potential values and plating current densities as a function of the $ZnSO_4$ concentration in the bath. The overall plating current density, i_{pl}, decreases, while the mixed potential shifts in the positive direction with the increase of $ZnSO_4$ concentration in the electrolyte. The calculated currents do not include the current due to the hydrogen evolution reaction. The model and the experimental data indicated that the addition of zinc ions inhibits the alloy deposition rate.

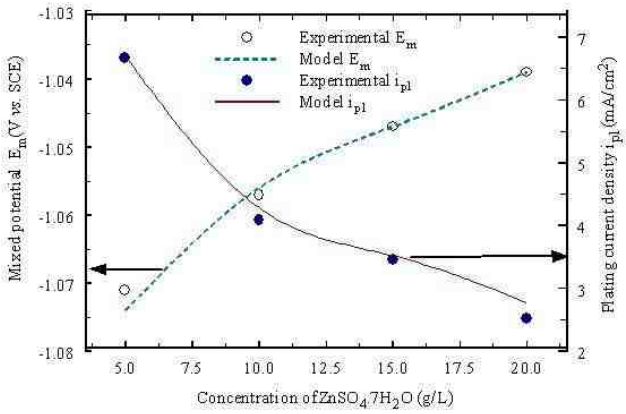

Figure 4 - Comparison of mixed potential E_m and plating current density i_{pl} obtained from the model and the experiments as a function of $ZnSO_4$ con-centration in the bath.

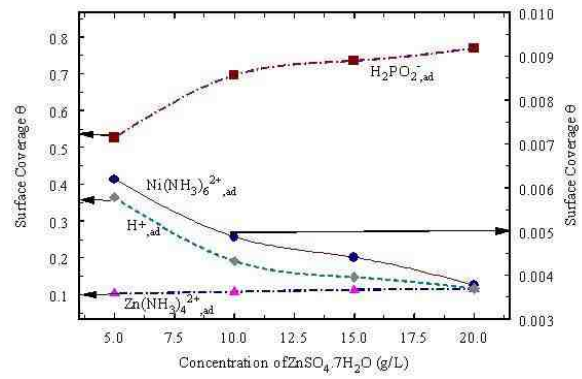

Figure 5 - Variation in surface coverages of the different reacting species as a function of $ZnSO_4$ concentration in the bath.

Figure 5 shows the surface coverage of all electroactive species participating in the deposition process as a function of $ZnSO_4$ concentration in the bath, as predicted by the model. By increasing the Zn ion concentration in the bath, the surface coverage of Ni ions decreases while the Zn ions surface coverage increases. This observation is in agreement with the results presented in Fig. 3. However, in Fig. 5, the surface coverage of hypophosphite ions increases with an increase of zinc ion concentration in the bath, which does not agree with the overall plating current density, i_{pl}, decrease observed in Fig. 4. In other words, one can expect an increase in the overall current density with an increase in hypophosphite ion surface coverage. The results can be explained by taking into account that the effective exchange current density for hypophosphite oxidation is also controlled by the square of the hydrogen ion surface coverage, Eq. (13).[60] The increase in hypophosphite ion concentration results in a decrease of hydrogen ion surface coverage, thereby reducing the effective exchange current density for hypophosphite oxidation. The effective exchange current density for hypophosphite decreases from 4.9×10^{-7} A/cm^2 to 6.7×10^{-8} A/cm^2 when the Zn ion concentration is increased from 5 g/L to 20 g/L. This results in reducing the current for hypophosphite oxidation, thus reducing the overall plating current density.

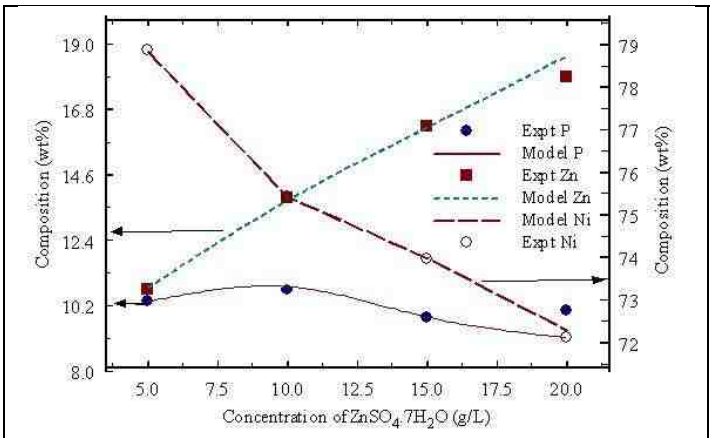

Figure 6 - Variation in Ni, Zn and P content as a function of $ZnSO_4$ concentration in the bath.

Figure 6 compares the model and experimentally estimated alloy compositions as a function of $ZnSO_4$ concentration in the electrolyte and is in agreement with the observations discussed in Figs. 4 and 5. The thickness of the deposits was checked using cross-sectional SEM analysis.[61]

Figure 7 shows the cross-sectional SEM pictures of Ni-P and Ni-Zn-P coatings when 5 g/L $ZnSO_4$ is added in the bath. The figure shows a decrease in the thickness of the final coating. The thickness decreases from 15.6 µm for the Ni-P coating to 10.2 µm for the Ni-Zn-P coating.

However, as a result of higher deposition potential for zinc deposition in alkaline electrolytes and a low overall plating mixed potential of -1.05 V_{SCE} estimated for the alloy deposition, the Ni-Zn-P alloy composition is high in Ni content. By increasing the zinc concentration and by controlling the concentration of the complexing agent, one can deposit the Ni-Zn-P alloy with a composition of 74:16:10 wt%. The corrosion and mechanical properties of this alloy are compared in the next section to those of zinc, cadmium, Zn-Ni (80:20 wt%),[68] Ni-Zn-Cd (50:40:10 wt%)[65] and Ni-Zn (68:32 wt%)[67] deposited from alkaline electrolytes.

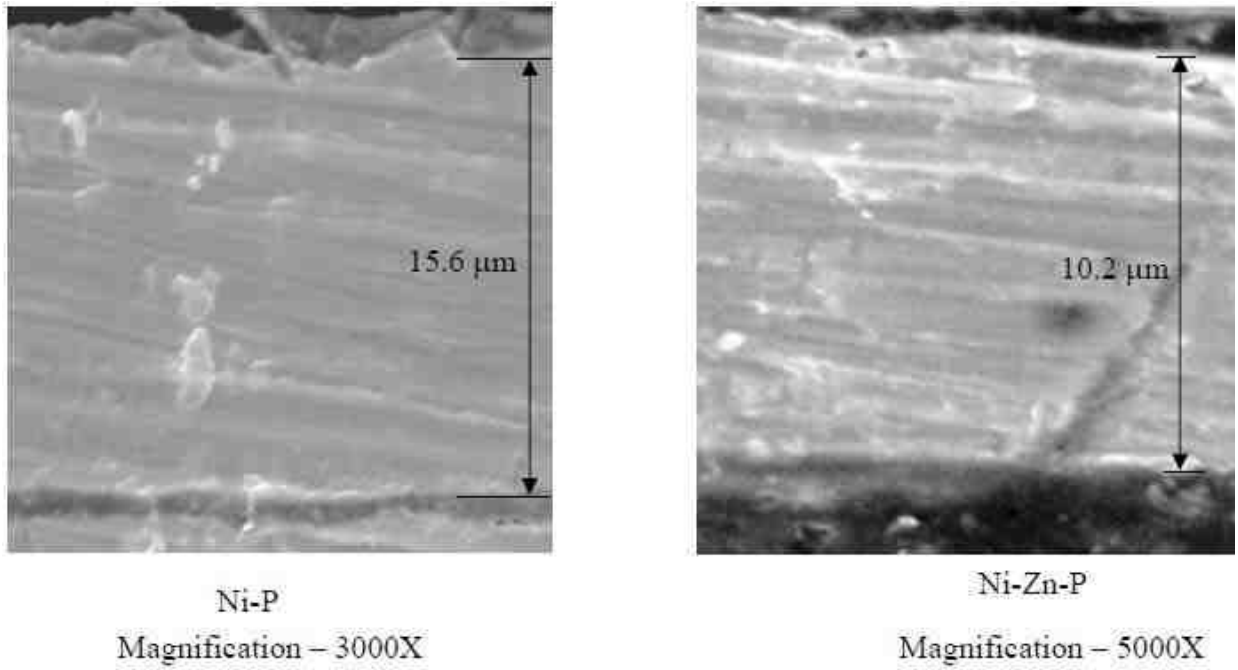

Figure 7 - Cross-sectional SEM pictures of the Ni-P and Ni-Zn-P coatings (prepared with 5g/L $ZnSO_4 \cdot 7H_2O$) for determining the thickness of the coatings.

Corrosion properties of Zn-Ni-X (X=P,Cd)

Table 1 -Corrosion properties of different sacrificial coatings determined by linear and Tafel polarization studies.

Coating	Composition (wt%)				E_{corr}, V_{SCE}	I_{corr}, A/cm^2	Corrosion rate × 10^{-10} cm/sec
	Zn	Ni	P	Cd			
Zn	100	-	-	-	-1.123	1.5×10^{-3}	39.4
Zn-Ni	94.6	5.4	-	-	-1.083	3.8×10^{-4}	17.7
Cd	-	-	-	100	-0.798	9.5×10^{-5}	17.2
Zn-Ni-Cd	49.6	20.8	29.6	-	-0.635	1.2×10^{-5}	5.1
Ni-Zn-P	16.2	74.0	9.8	-	-0.652	8.5×10^{-6}	3.3
Ni-Zn	28.0	72.0	-	-	-0.678	4.8×10^{-6}	2.9

Table 1 shows various coatings that have been chosen for comparison along with the E_{corr} values and corrosion currents. All the corrosion studies were performed in a solution of 0.5M Na_2SO_4 and 0.5M H_3BO_3, pH = 7.0. The corrosion rates were calculated using the polarization resistance estimated from the linear polarization technique. Figure 8 summarizes the corrosion rates obtained for various coatings in the form of a bar plot which indicates the superior corrosion properties of Zn-Ni-Cd, alkaline Ni-Zn[67] and Ni-Zn-P[61] (electroless) coatings. Figure 9 presents a comparison of Nyquist responses obtained for Zn, Zn-Ni,[68] Cd, Zn-Ni-Cd, electrolytic Ni-Zn and electroless Ni-Zn-P coatings. The electrodeposited Ni-Zn alloy and electroless Ni-Zn-P offer a barrier resistance in the order of 2000 Ω, which is five times higher than the typical Cd deposit. The increase in the barrier resistance of these coatings is an outcome of the increase of the nickel content in the deposit.

The sacrificial properties, as predicted by the OCP measurements, were verified using the scratch-model approach. The more electronegative zinc coatings offer a higher level of sacrificial protection to the underlying steel and inhibit the hydrogen penetration in the bulk of the alloy.[61] However, this coating has a very short life due to a high rate of galvanic corrosion. The potential of pure zinc was stable at –1.1 V_{SCE} whereas, the OCPs of Zn-Ni and Zn-Ni-Cd, Ni-Zn and electroless Ni-Zn-P were more positive, indicating that inclusion of more noble components in the deposit results in the anodic shift in potentials with respect to zinc which in turn decreases the galvanic corrosion. The potentials of Zn, Zn-Ni, Cd, Zn-Ni-Cd, alkaline Ni-Zn and Ni-Zn-P deposits were continuously monitored with respect to SCE as a function of time. The results presented as potential-time plateaus are shown in Fig. 10. The OCP plots of Zn-Ni showed three distinct plateaus occurring at three different potentials namely, -1000 mV_{SCE}, -700 mV_{SCE} and –400 mV_{SCE}. The observed plateaus correspond to different phases of Zn-Ni. Zn-Ni alloys deposit in three phases, a Zn-rich phase called eta (η) phase (E_{corr} = -1.050 V_{SCE}), an intermediate gamma (γ) phase, (E_{corr} = -0.700 V_{SCE}) and a nickel rich alpha (α) phase (E_{corr}= -0.400 V_{SCE}). The plot shows that the commercially available coatings such as Zn, Zn-Ni and cadmium corrode for less than 60 hr. On the other hand the Ni-Zn and electroless Ni-Zn-P alloys have prolonged life of more than 100 hr. Alkaline electrolytic Ni-Zn and amorphous nanosized Ni-Zn–P coatings were tested in the Naval Aviation Center (NAVAIR) as a substitute for cadmium coatings. One of the primary requirements for the substitution of cadmium is that no signs of white rust or red rust should be found after 96 hr in an unscribed and scribed salt fog testing as per ASTM B117-94 specifications. The scribed salt showed no rust in the scribed area for the electrolytic alkaline Ni-Zn and multilayered nanosized amorphous Ni-Zn-P coatings.

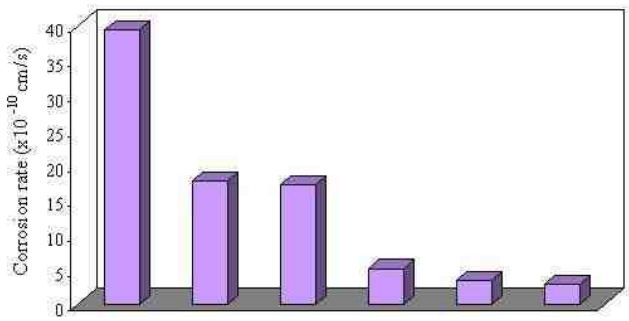

Figure 8 - Comparison of linear polarization plots for Zn, Zn-Ni, Cd, Zn-Ni-Cd, electroless Ni-Zn-P and alkaline Ni-Zn coatings.

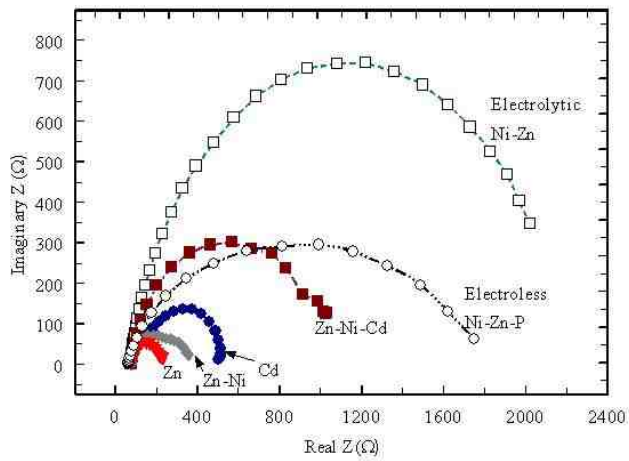

Figure 9 - Nyquist responses of the various sacrificial coatings.

Mechanical properties

Table 2 summarizes the mechanical properties of the various coatings tested along with their compositions obtained using EDAX analysis. Table 2 indicates that the hardness of Ni-Zn-P alloys is comparable to that of Cd coatings. The reason for this higher hardness of Ni-Zn-P versus Zn-Ni alloy is due to the increased amount of Ni in the alloy.[67,68] Thus, the results indicated that Ni-Zn-P alloys possess engineering attributes similar to those of Cd coatings.

Table 2 - Comparison of mechanical properties for the various sacrificial coatings.

Coating	Adhesion	Taber Wear Index (mg)	Microhardness (HK_{25})
Zn	Good	29.7	82
Zn-Ni	Mild Flaking	18.5	105
Cd	Good	6.0	240
Ni-Zn-P	Good	8.0	198

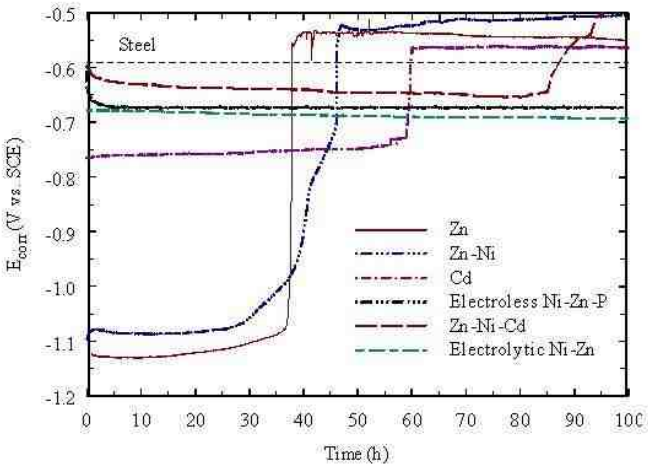

Figure 10 - E_{corr} vs. time plot for the various alloy coatings (thickness = 2 μm) immersed in 0.5M Na_2SO_4 and 0.5M H_3BO_3 (pH=7.0).

Pulse plating of nano-sized Pt coatings

Polymer Electrolyte Membrane (PEM) fuel cells offer low weight and high power density and are being considered for automotive and stationary power applications.[69-72] State-of-the-art PEM fuel cells use a five-layer structure consisting of the anode, cathode, a membrane separating the two electrodes and two gas diffusion layers on one end of each of the electrodes. Among these, the membrane electrode assembly (MEA) comprising the anode, cathode and membrane is the key component in the PEM fuel cell. The proton exchange membrane in the middle separates the electrodes to prevent an electrical short. The PEM fuel cell operates at 80 to 120°C and at this temperature the hydrogen oxidation and oxygen reduction rates are low. Hence, platinum catalysts are used to enhance the reaction rates. Use of platinum catalysts increases the cost thus necessitating the reduction of Pt loading. Current approaches to prepare MEAs can be broadly divided into two different categories: powder type and non-powder type. The powder type involves the process of catalyzation on a high surface area of carbon using Pt catalyst.[73-77] The prepared carbon supported catalyst is applied to the membrane followed by GDL (gas diffusion layer) additions to the GDL followed by membrane addition.

For the powder type based methods, it is difficult to control the particle size of the catalyst when the platinum-to-carbon ratio increases to more than 40 wt%. In order to overcome this limitation, several non-powder type processes were developed. These processes (two step impregnation-reduction,[78] evaporative deposition,[79] sputtering[80]) have focused on localizing the catalyst near the surface of the electrode or directly on membrane in order to increase the contact between catalyst and membrane.[78-80] However, these technique are not volume production methods.

As a non-powder type technique, electrodeposition has attracted attention because of its ease of preparation and low cost requirements. Taylor, *et al.*[81] developed an electrochemical catalyzation (ECC) technique to improve the utilization of Pt catalyst. In this technique, gas diffusion electrodes were prepared from uncatalyzed carbon. Later Nafion® was impregnated into the electrode and the Pt catalyst was electrodeposited though the Nafion® into the electrode from a commercial plating bath. In this process, Pt was deposited only in the regions of ionic and electronic conductivity. This increased the Pt utilization and hence reduced the loading to 0.05 mg Pt/cm^2. The ECC electrodes showed almost the same performance as the standard 10% Pt/C electrode made from platinum colloid followed by Nafion® impregnation. Also they showed a 10-fold increase in mass activity compared to the standard electrodes. A selective localized electrodeposition of the catalyst within the active layer of the membrane-electrode assembly has been also suggested in the literature.[82-84]

A new approach based on pulse electrodeposition to prepare MEAs was developed in our laboratories which increases the efficiency of MEAs by decreasing the particle size and localizing the catalyst near the membrane.[85] Pulse plating has traditionally been shown to produce deposits with lower grain sizes and particle sizes as compared to DC plating.[86,87] For MEAs, this method has the potential to create Pt particles smaller than 5 nm while generating a high Pt/C ratio at the membrane-electrode interface. Further, this technique ensures that most of the platinum is in close contact with the membrane. By placing a smaller particle of platinum on the surface of the electrode, the MEA prepared by this method shows higher performance with a smaller amount of Pt than conventional electrodes.

In an electroplating process, metal ions are transferred to the cathode, and adatoms are formed by the charge transfer reaction and finally incorporated into the crystal lattice. This occurs by building up existing crystals (growth of crystals) or creating a new one (nucleation). These two steps are in competition and can be influenced by the surface diffusion rate of adatoms and the rate of charge transfer reaction. High surface diffusion rates, low population of adatoms caused by slow charge transfer reaction and low overpotentials lead to the growth of crystals, while conversely low surface diffusion rates, high population of adatoms and high overpotentials increase the rate of nucleation.[87] The nucleation rate[88] is given by:

$$J = K_1 \exp\left[\frac{-bs\varepsilon^2}{zekT\eta}\right] \tag{19}$$

where K_1 is the rate constant, b is the geometric factor depending on the shape of the 2D cluster ($b = P^2/4S$, where P is the perimeter and S is the surface area), s is the area occupied by one atom on the surface of the nucleus, ε is the edge energy, k is the Boltzmann constant, z is the electronic charge of the ion, e is the charge of the electron, T is the temperature. The overpotential, η, is given by the Tafel expression,

$$\eta = \alpha + \beta \log i \tag{20}$$

where α and β are constants and i is the current density. From the above equations it can be seen that as the applied current increases as the overpotential increases, which in turn according to Eq. (10), the critical radius decreases and the nucleation rate increases.

It is generally reported as an advantage of pulse electrodeposition that a higher cathodic current density for deposition can be applied to the plating system due to the higher concentration of metal ions at the surface of the electrode in contrast to applying a direct current (DC). In an attempt to develop theoretical interpretations of pulse and DC deposition processes, a simple diffusion model was suggested.[89,90] The current wave form of pulse deposition used is shown in Fig. 11. Unlike DC electrodeposition, pulse electrodeposition has three independent variables, namely, on time (θ_1), off time (θ_2) and peak current density (i_p). The duty cycle is defined as follows:

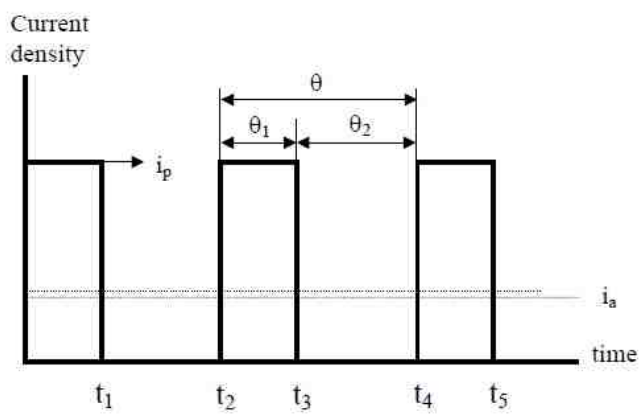

Figure 11 - Current waveform and parameters of pulse electro-deposition.

$$\text{Duty cycle (\%)} = \frac{\theta_1}{\theta_1 + \theta_2} \times 100 \tag{21}$$

The average current density (i_a) can be calculated from peak current density and the duty cycle. The ratio of the limiting current density in pulse electrodeposition $(i_p)_l$ and DC plating $(i_{dc})_l$ is given below:

$$\frac{(i_p)_l}{(i_{dc})_l} = \frac{1}{1 - \frac{8}{\pi^2}\sum_{j=1}^{\infty}\frac{1}{(2j-1)^2}\cdot\frac{\left(\exp\left[(2j-1)^2 a\theta_2\right]-1\right)}{\left(\exp\left[(2j-1)^2 a\theta\right]-1\right)}} \tag{22}$$

where $a = \pi^2 D / 4\delta^2$ (sec^{-1}) is the diffusion parameter, D is the diffusion coefficient (cm^2/sec) while δ is the thickness of the diffusion layer (cm). This ratio for various values of $a\theta$ (pulse period) and θ_1/θ (duty cycle) are plotted in Fig. 12. The result shows that the limiting current density of pulse electrodeposition is always higher than DC electrodeposition. And the electrodeposition can be carried out at a higher current density by decreasing the pulse periods or by decreasing the duty cycle. According to Eq. 20, the larger the current density, the higher the overpotential. Thus, the nucleation rate increased, resulting in a finer crystal grain.

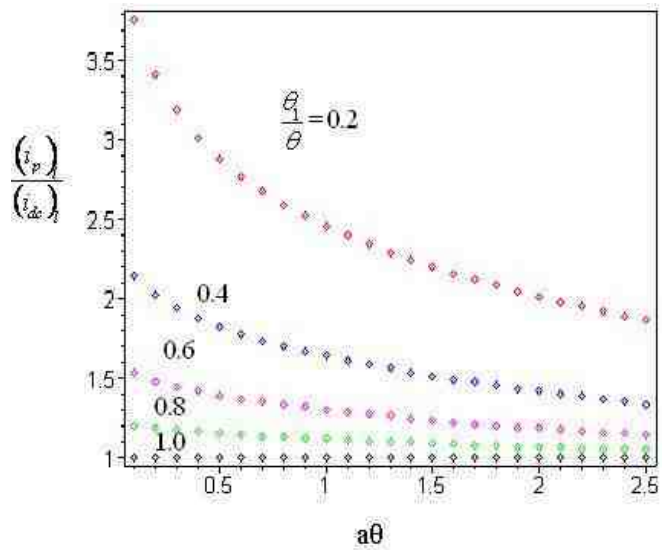

Figure 12 - Ratio of limiting current density between pulse and DC electrodeposition as a function of duty cycles.

Figure 13(a) displays the back-scattered electron image of the cross-section of an MEA consisting of a commercial anode and pulse deposited cathode** in our laboratories. This image shows the five layers clearly and is useful for identifying the thickness of the membrane, catalyst layer and gas diffusion electrode regions. The thickness of the Nafion® membrane is confirmed to be 50 µm according to the scaling bar given in the bottom of the picture. The bright portion between the membrane and gas diffusion layer is associated with the presence of the heavier element such as Pt. Thus, these two light colored bands on either side of the membrane show the thickness of the electrocatalyst layer on the anode and cathode side. The most striking aspect of this image is that the thickness of the pulse electrodeposited Pt electrocatalyst layer is only 5 µm, which is ten times thinner than that of the commercial electrode. This is also confirmed from the concentration profile of Pt measured across a typical portion of the cross section of the MEA by a line scan using EPMA [see Figure 13(b)]. It is useful here to distinguish between the two different approaches used to prepare the anode and cathode. The commercial anode was prepared using the conventional powder type

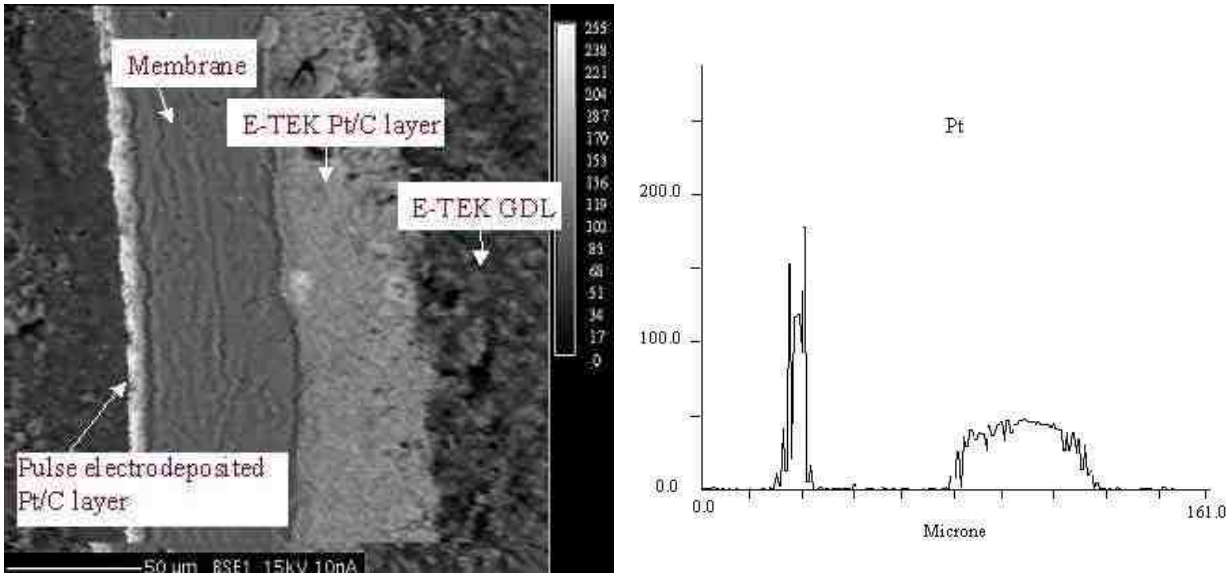

Figure 13 - (a) Back-scattered electron image and (b) Pt line scan of the cross section of MEA using EPMA.

**E-TEK commercial electrodes, E-TEK Div. of De Nora N.A., Inc., Somerset, NJ 08873-6800.

approach where Pt/C mixture is dispersed and then loaded on the gas diffusion layer by spraying or coating. The cathode was prepared by the pulse electrodeposition approach, by plating Pt on the carbon support and subsequently attaching it to the Nafion® membrane. In Figure 13(b), the pulse electrodeposited cathode exhibits a much higher intensity of the Pt peak in the limited area near the membrane while the Pt line scan across the commercial anode electrode shows a relatively uniform intensity with a thickness of 50 µm. It is also seen that the anode thickness is much more than that of the cathode.

In order to quantify the Pt ratio in the catalyst layer, EDX spot analysis coupled with ESEM was also carried out for this cross section of the MEA. Figure 14 shows the concentration distribution of Pt in the electrocatalyst layer of the commercial Pt/C layer and pulse electrodeposited Pt/C cathode with a distance from the membrane. According to this analysis, the content of Pt in the cathode catalyst layer prepared by pulse electrodeposition, decays with increasing distance from the membrane to the GDL. The Pt to carbon ratio at 1 µm distance from the membrane is about 75 wt%, and this value reduces to almost zero at a distance of 7 µm from the membrane. In contrast, the commercial electrode shows about 20 wt% of Pt/C ratio distributed uniformly over the entire range of the catalyst layer. Both experimental and modeling studies of membrane electrodes indicate that active layers thicker than 10 µm result in low catalyst utilization due to transport limitations of dissolved oxygen and protons in the ionomer.[92] It thus appears that pulse deposition is an attractive technique to replace the conventional powder type MEA preparation methods and help achieve industry goals of reducing catalyst cost and increasing efficiency in PEM fuel cells.

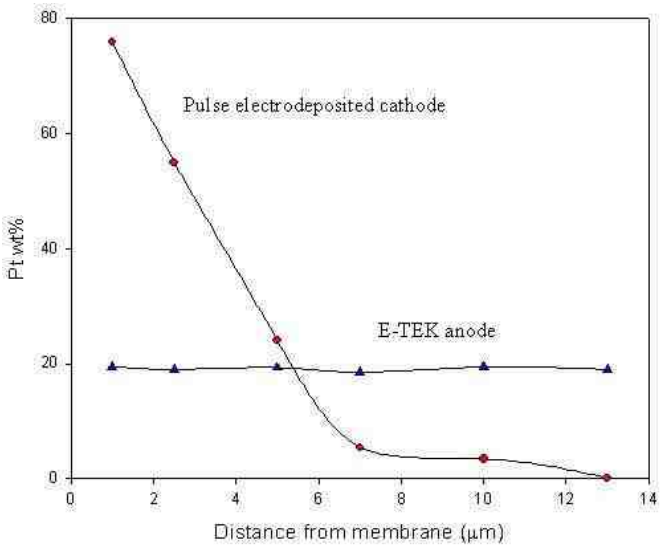

Figure 14 - Pt concentration profile of the cross-section of MEA using EDX spot analysis.

Figure 15 shows a typical TEM image of a catalyst prepared by pulse electrodeposition. From the low magnitude TEM image noted as (A), the dark spot indicates the presence of platinum and the light one indicates presence of carbon. The scaling bar of 100 nm is given at the bottom of the image. According to this data, the particle size of carbon is 60 to 70 nm, and the particle size of platinum seems to be smaller. So it would be a reasonable guess that a much smaller particle of platinum deposits on the surface of carbon and for this reason, both particle sizes look similar. Next, the TEM magnification was increased to 400,000X. The TEM image as shown in Fig. 15(B) indicates that the large dark particles consist of small particles in the range of 3~4nm.

Because, in our approach, only one side of the carbon was exposed to the electrolyte, Fig. 15 clearly illustrates that only one side of the carbon particle has platinum while the other side is not covered. It is obvious that Pt metal particles only exist very close to the surface of the electrode and that a very thin nanostructured catalyst layer was obtained from the pulse electrodeposition approach.

Figure 16 shows the polarization curves of the PEM fuel cell prepared by direct current (DC) and pulse current (PC) electrodeposition of Pt. The conditions of pulse electrodeposition are 200 mA/cm^2 of peak current density, 5.2 msec on time and 70 msec off time. Total charge is fixed at 6 Coulomb/cm^2 on both cases. This data clearly shows the advantage of pulse electrodeposition. The MEA prepared by pulse electrodeposition of higher current density exhibits a much higher performance compared to the MEA by direct current deposition at lower current density. This difference in performance can be accounted for by changes in Pt particle size. In order to optimize the particle size and improve MEA performance, studies varying the pulse plating conditions were done. In the case of PC deposition, metal ions diffused into the surface of the electrode during the off time so that it is possible for the electrodeposition to be carried out at higher peak current density. However, DC deposition continuously consumes metal ions without refilling. A performance comparison between the pulse electrodeposited electrode and the commercial electrode in Fig. 17 shows the performance of the PEM fuel cell using two different types of cathode. One was prepared using our selective deposition method and the other prepared using a conventional colloidal method. The

deposition condition is that the peak current density is 200 mA/cm^2, on time is 5 msec, off time is 102.8 msec and total charge density is 11 Coulomb/cm^2. The selective deposition of Pt, according to our method, leads to higher current densities at a given potential.

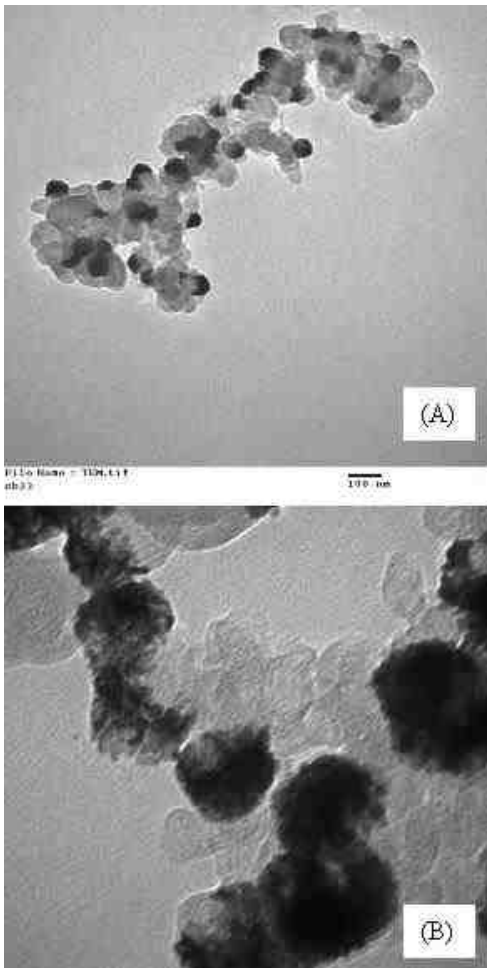

Figure 15 - TEM image of the Pt supported on carbon electrode prepared by pulse electrodeposition magnified at (A) 100,000X and (B) 400,000X.

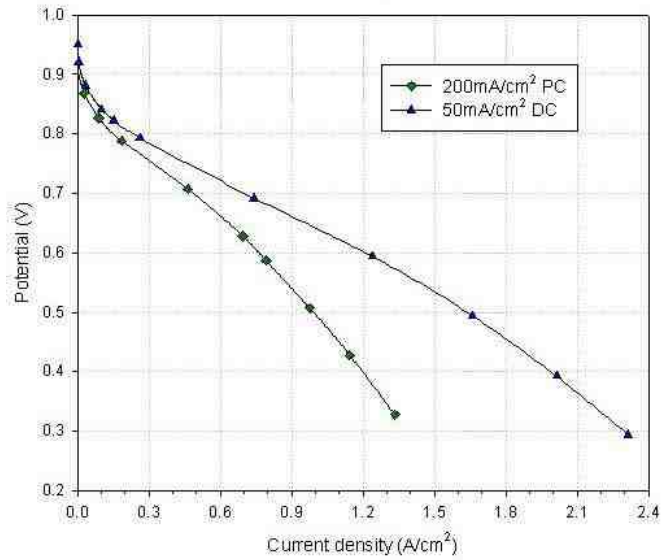

Figure 16 - Polarization curves of MEAs prepared by direct current and pulse electrodeposition.

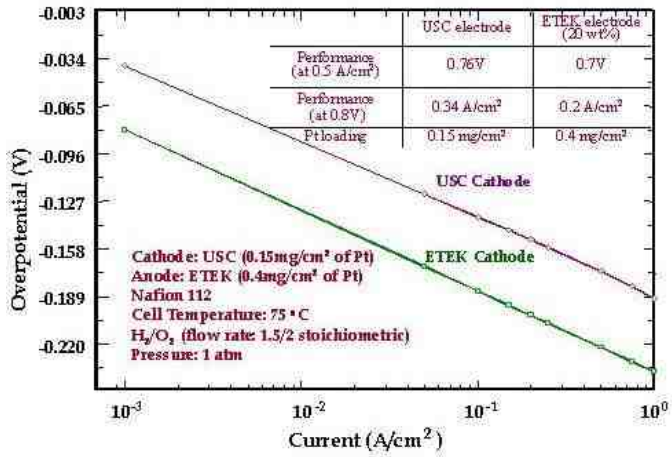

Figure 17 - Comparison of performance between a pulse electrodeposited electrode and a commercial electrode.

Concluding remarks

Novel techniques for the deposition of non-anomalous amorphous Ni-Zn-P, crystalline Ni-Zn and Zn-Ni-Cd have been developed for protection of steel. These coatings show promise as a replacement for Cd in sacrificial protecting steel. By decreasing the Zn-Ni ratio in the above alloys, their corrosion potential decreases from initial value of -1.14 V_{SCE} observed for anomalous Zn-Ni alloy to corrosion potentials lower than that of Cd (-0.79 V_{SCE}). Also by introducing a third element in the alloy, it was possible to modify the rate of the hydrogen evolution reaction, the hydrogen proton recombination and adsorption kinetics at the surface and to inhibit the corrosion and hydrogen permeation. The role of current distribution, mass transfer and charge transfer kinetics have been identified and demonstrated on the autocatalytic deposition of Ni-Zn-P alloy from alkaline electrolytes by using mixed potential theory. It was found that this deposition technique can be optimized by considering the equilibrium concentrations of all complexes formed in the bath and coupling the charge transfer reactions through adsorbed species at the electrode-electrolyte interface. It was

shown that the model can optimize the chemical composition and the depositing parameters which gives a valuable tool to the experimentalist to control the alloy functional properties.

This paper provided evidence that a novel pulse electrodeposition technique was developed as a new method for fabricating MEAs. In our approach, nanostructured platinum is directly deposited on the hydrophilic surface of a carbon electrode. This ensures that most of the platinum is in close contact with the membrane. With increasing peak current density, the particle size of platinum decreased and the performance of the MEA increased. The increased current density increases the overpotential of deposition, resulting in the increase of nucleation rate. By optimizing the pulse deposition conditions, it was found that the 3-4 nm particle size of platinum could be prepared with a very thin catalyst layer thickness. The Pt/C ratio could be increased to 75 wt% near to the surface of electrode resulting in 5 μm of catalyst layer thickness while the commercial electrode prepared by colloidal method showed 50 μm catalyst thickness. By placing a smaller particle of platinum on the surface of electrode, the MEA prepared by pulse electrodeposition technique shows higher performance with smaller amount of Pt than the commerical elelctrode prepared by the conventional method.

Acknowledgments.

Financial support by AESF Research Contract Project 107, Dr. John Sedriks, Office of Naval Research under grant no. N00014-00-1-0053 and UTC Fuel Cells are gratefully acknowledged.

References

1. P. Subramanyan in *Comprehensive Treatise of Electrochemistry*, J.O'M. Bockris, B.E. Conway, E. Yeager & R.E. White, Eds., Vol. 2, Plenum Press, New York, NY, 1981; p .411.
2. S. Raskov, C. Boskov, V. Kudrajavtsev, S. Bagaev & K. Pedan, *J. Electronal. Chem*., 248, 241 (1988).
3. J-M. Chen & J.-K Wu, *Plating & Surface Finishing,* 79, 74 (October 1992).
4. J-M. Chen & J.-K Wu, *Corros. Sci.,* 33, 657 (1992).
5. G. Zheng, B.N. Popov & R.E. White, *J. Electrochem. Soc.,* 140, 3153 (1993).
6. B.N. Popov, G. Zheng & R.E. White, *Corrosion*, 50, 613 (1994).
7. B.N. Popov, G. Zheng & R.E. White, *Corrosion Science*, 36, 2139 (1994).
8. G. Zheng, B.N. Popov & R.E. White, *J. Electrochem. Soc.*, 141, 1526 (1994).
9. G. Zheng, B.N. Popov & R.E. White, *J. Electrochem. Soc.,* 141, 1220 (1994).
10. B.N. Popov, G. Zheng & R.E. White, *Corrosion*, 51, 429 (1995).
11. G. Zheng, B.N. Popov & R.E. White, *J. Appl. Electroch.,* 25, 212 (1995).
12. G. Zheng, B.N. Popov & R.E. White, *J. Electrochem. Soc.,* 142, 154 (1995).
13. H.A. Duarte, B.N. Popov & R.E. White, *J. Electrochem. Soc.,* 144, 2313 (1997).
14. M. Ramasubramanian, B.N. Popov & R.E. White, *J. Electrochem. Soc.,* 145, 1907 (1998).
15. H.A. Duarte, D.M. See, B.N. Popov & R.E. White, *Corrosion,* 54, 187 (1998).
16. D.H. Coleman, B.N. Popov & R.E. White, *J. Electrochem. Soc.,* 143, 1871 (1996).
17. M.A. Devanathan & Z. Stachurski, *Proc. Royal Soc., London Ser. A,* 270, 90 (1962).
18. R.N. Iyer & H.W. Pickering, *Ann. Rev. Mater. Sci.,* 20, 299 (1990).
19. R.E. Marce, *Industrial Finishing,* 54, 34 (April 1978).
20. V.C.R. McLoughlin, *Trans. IMF,* 57, 102 (1979).
21. R. Walker, *Metal Finishing,* 72, 59 (Jan 1974).
22. A. Ashur, J. Sharon, I.E. Klein, *Plating & Surface Finishing,* 83, 58 (July 1996).
23. W.H. Safranek, *Plating & Surface Finishing,* 84, 45 (August 1997).
24, D. Altura, F. Mansfield & L.P. Streett, *Plating,* 61, 850 (1974).
25. A.J. Boehm, *Plating & Surface Finishing*, 80, 52 (April 1993).
26. J.A. Bates, *Plating & Surface Finishing,* 81, 36 (April 1994).
27. G. F. Hsu, *Plating & Surface Finishing,* 71, 52 (April 1984).
28. N. Zaki, *Metal Finishing,* 87, 57 (June 1989).
29. D.E. Hall, *Plating & Surface Finishing,* 70, 59 (November 1983).
30. K.R. Baldwin & C.J.E. Smith, *Product Finishing,* 45, 12 (June 1992).
31. K.R. Baldwin, M.J. Robinson & C. J.E. Smith, *Corrosion Science,* 35 (5-8), 1267 (1993).

32. *Plating, zinc-nickel alloy, Aerospace Material Specification 2417E, 1st January 1993*, SAE International, Warrendale, PA, 1993.
33. *Standard specifications for electrodeposited coatings for Zn-Ni alloys deposits, ASTM B841*, ASTM, Race St, Philadelphia, PA, 1994.
34. N.R. Short, A. Abibsi & J.K. Dennis, *Trans. IMF,* 67, 73 (1991).
35. *Standard Specification for Electrodeposited Coatings for Zn-Co alloys deposits, ASTM B840*, ASTM, Race St, Philadelphia, PA, 1994.
36. D.E. Lay & W.E. Eckles, *Plating & Surface Finishing,* 77, 10 (October 1990).
37. I. Kirilova, I. Ivanov & St. Rashkov, *J. Applied Electrochem.,* 27, 1380 (1997).
38. T. Tsuchida & I. Suzuki, U.S. patent 4,581,110 (1986).
39. International Tin Research Institute, *Product Finishing,* 47, 15 (February 1994).
40. M. Sagiyama, T. Urawaka, T. Adaniya & T. Hara, *Proceedings of the Conference on Coatings & Steel,* AESF, Orlando, FL, February 1986.
41. M. Eyraud, A. Garnier, F. Mazeron & J. Crousier, *Plating & Surface Finishing,* 82, 63 (January 1995).
42. W. H. Safranek, *The Properties of Electrodeposited Metals & Alloys*, AESF, Orlando, FL, 1986; p. 466.
43. A. Brenner, *Electrodeposition of Alloys, Principles & Practice,* Academic Press, New York, 1963.
44. N.S. Grigoryan, V.N. Kudryavtsev, P.A. Zhdan, I.Y. Kolotyrkin, E.A. Volynskaya & T. A. Vagramyan, *Zasch. Met.,* 25, 288 (1989).
45. A. Durairajan, B. Haran, R.E. White & B.N. Popov, *J. Electrochem. Soc.,* 147, 48 (2000).
46. A. Krishniyer, M. Ramasubramanian, B.N. Popov & R.E. White, *Plating & Surface Finishing,* 86, 99 (January 1999).
47. A. Durairajan, A. Krishniyer, B. Haran, R.E. White & B.N. Popov, *Corrosion*, 56, 283 (2000).
48. A. Durairajan, B. Haran, R.E. White & B.N. Popov, *J. Electrochem. Soc.,* 147, 48 (2000).
49. A. Durairajan, Ph.D. Thesis , University of South Carolina, Columbia, SC. 2001.
50. Z. Zhou, T.J. O'Keefe, *Surface & Coatings Technology*, 96, 191 (1997).
51. B.N. Popov, D. Slavkov, T. Grcev, Lj. Arsov & S. Kariavanov, *Kem. Ind.,* 1, 1 (1986).
52. B.N. Popov, M. Ramasubramanian, S.N. Popova, R.E. White & K-M. Yin, *J. Chem. Soc., Faraday Trans.,* 92, 4021 (1996).
53. J.C. Puippe in *Theory & Practice of Pulse Plating,* J. C. Puippe & F. Leaman, Eds., AESF, Orlando, FL, 1986; p17.
54. K. Kondo, T. Sagawa & K. Shinohara, *J. Electrochem. Soc.,* 142, L193 (1995).
55. A. Takahashi, Y. Miyoshi & T. Hada, *J. Electrochem. Soc.,* 141, 954 (1994).
56. K.R. Baldwin, M.J. Robinson & C J.E. Smith, *British Corrosion Journal,* 29, 299 (1994).
57. M. Bouanani, F. Cherkaoui, R. Fratesi, G. Roventi, G. Barucca, *J. Appl. Electrochem.,* 29, 637 (1999).
58. E. Valova, I. Georgiev, S. Armyanov, J.-L. Delplancke, D. Tachev, Ts. Tsacheva & J. Dille, *J. Electrochem. Soc.,* 148, C266 (2001).
59. M. Schlesinger, X. Meng & D.D. Snyder, *J. Electrochem. Soc.,* 138, 406 (1991).
60. B. Veeraraghavan, K. Hansung & B.N. Popov, *Electrochimica Acta,* 49, 3143 (2004).
61. B. Veeraraghavan, B. Haran, S.P. Kumaraguru & B. Popov, *J. Electrochem. Soc.,* 150, B151 (2003).
62. I. Ohno & S. Haruyama, *Sur. Technol.,* 13, 1 (1981).
63. W.M. Latimer, *Oxidation states of the elements and their potentials in aqueous solutions,* Prentice-Hall Inc., New York (1952).
64. M. Wasberg & G. Horanyi, *Electrochim. Acta.*, 40, 615 (1995).
65. H. Kim, B.N. Popov & K.S. Chen, *Corrosion Science*, 45, 1505 (2003).
66. H. Kim, B.N. Popov & K.S. Chen, *J. Electrochem. Soc.,* 150, C81 (2003).
67. S.P. Kumaraguru & B.N. Popov, *J. Appl. Electrochem.,* Submitted for publication.
68. D.H. Coleman, B.N. Popov & R.E. White, *J. Appl. Electrochem.*, 28, 889 (1998).
69. R. Gonzalez & S. Srinivasan, *J. Hydrogen Energy*, 9, 215 (1984).
70. K.B. Prater, *J. Power Sources,* 61, 105 (1996).
71. S.G. Chalk, J.F. Miller & F.W. Wagner, *J. Power Sources*, 86, 40 (2000).
72. D. Rastler, *J. Power Sources*, 86, 34 (2000).
73. S. Srinivasan, A. Ferreira, R. Mosdale, S. Mukerjee, J. Kim, S. Hirano, S. Lee & F. Buchi, A. 84. Appleby, in: *Proceedings of the Fuel Cell*, 424 (1994).
74. S. Gottesfeld & M. Wilson, *J. Electrochem. Soc.*, 139, L28 (1992).
75. S. Gottesfeld & M. Wilson, *J. Appl. Electrochem.*, 22, 1 (1992).
76. M. Uchida, Y. Aoyama, N. Eda & A. Ohta, *J. Electrochem. Soc.*, 142, 463 (1995).
77. E. Gulzow, M. Schulze, N. Wagner, T. Kaz, R. Reissner, G. Steinhilber & A. Schneider, *J. Power Sources,* 86, 352 (2000).

78. P.S. Fedkiw & W-H. Her, *J. Electrochem. Soc.*, 136, 899 (1989).
79. S. Foster, P. Mitchell & R. Mortimer, in *Proceedings of the Fuel Cell*, 442 (1994).
80. S. Hirano, J. Kim & S. Srinivasan, *Electrochim. Acta*, 42, 1587 (1997).
81. E.J. Taylor, E.B. Anderson & N.R.K. Vilambi, *J. Electrochem. Soc.*, 139, L45 (1992).
82. M.W. Verbrugge, *J. Electrochem. Soc.,* 141, 46 (1994).
83. O. Antoine & R. Durand, *Electrochem. Solid-State Lett*., 4, A55 (2001).
84. T.J. Schmidt, U.A. Paulus, H.A. Gasteiger & R.J. Behm, *J. Electroanal. Chem*., 508, 41 (2001).
85. H. Kim & B.N. Popov, *J. Electrochem. Soc.,* submitted for publication.
86. N.A. Qu, D. Zhu, K.C. Chan & W.N. Lei, *Surface & Coatings Techno*logy, 168, 123 (2003).
87. E. Budevski, G. Staikov & W.J. Lorenz, *Electrochem. Acta*, 45, 2559 (2000).
88. J. Puippe & F. Leaman, *Theory & Practice of Pulse Plating*, AESF, Orlando, FL, 1986.
89. M. Paunovic & M. Schlesinger, *Fundamentals of Electrochemical Deposition*, Electrochemical Society Series, Electrochemical Society, Pennington, NJ, 1998.
90. H.Y. Cheh, *J. Electrochem. Soc.,* 118, 551 (1971).

About the author

This is an edited version of documentation provided to the Scientific Achievement Award Committee on Dr. Popov's achievements.

The Scientific Achievement Award is the Society's most prestigious award. Its purpose is to recognize those whose outstanding scientific contributions have advanced the theory and practice of electroplating, metal finishing and allied arts; have raised the quality of products and processes; or have advanced the dignity and status of the profession.

Each year at SUR/FIN, the Scientific Achievement Award Committee meets to deliberate the achievements of individuals nominated for the award. The Committee's selection as the 2002 recipient is Dr. Branko N. Popov, professor of chemical engineering, Department of Chemical Engineering, University of South Carolina, Columbia, SC.

Dr. Popov has published more than 70 articles in refereed journals in the area of theory and practice of electroplating and metal finishing. He's a 1999 Abner Brenner Award winner (for an outstanding paper published in *P&SF*). His research work has been supported by the AESF, the United Nations (UN), Macedonian Science Foundation (MSF), Army Research Office (ARO), Office of Naval Research (ONR), the Department of Energy (DOE), National Science Foundation (NSF), and Sandia National Laboratories.

Throughout his 37-year career, Dr. Popov has been affiliated with well-known universities: University Kiril & Metodij, Skopje, Macedonia; the University of Illinois; Texas A&M University; and the University of South Carolina. He has taught courses in electrochemistry, corrosion and corrosion control, physical chemistry, chemical thermodynamics, chemical and electrochemical kinetics, and electrochemical DC and AC methods for corrosion rate determinations and electrochemical processes.

Contributions to the Advancement of the Theory & Practice of Plating & Metal Finishing

With more than 70 papers published in the last 10 years in the area of electrodeposition, Dr. Popov has made crucial advancements in the theory and practice of plating and metal finishing. The theoretical work in the area of electrochemical deposition and corrosion engineering includes development of new technologies and treatments for underpotential deposition of Zn, Bi, Pb Ti and Pb, and deposition of secondary, ternary and quaternary alloys that inhibit corrosion and prevent hydrogen embrittlement of the substrates.

New treatments were developed for underpotential deposition of Zn, Ni, Bi and Pb on steel substrates, which inhibited the hydrogen evolution and penetration through AISI 4340 steel, HY 130 steel, Inconel 718, and Monel K500.

Procedures for deposition of nano-structured multi-barrier layers of Bi, Zn and Zn-Ni (10-11 nm each) were developed for the ONR. For the Zn, Zn-Ni and Bi electroplates, hydrogen evolution and permeation decreased with each successive layer until reaching an average of 99% inhibition when compared with bare iron. The theoretical models developed to explain the processes at the electrode/electrolyte inerface indicated that the decrease in the permeation rate of hydrogen through the substrate was attributed to the decrease of hydrogen discharge rate and suppression of hydrogen absorption on the deposited layers.

Dr. Popov & AESF Research

Dr. Popov has been continuously supported by the AESF Research Program since 1990. The objectives of the projects were to develop a technology for the electrodeposition of Fe-Ni, Zn-Ni-P alloys and Zn-Ni-SiO ternary alloys, and to characterize the deposition as a function of various additives in the electroplating bath. The depositions were studied as a function of various organic and inorganic additives in the bath. The corrosion resistance of the alloys deposited was determined as a function of the deposition conditions. A theoretical model was developed that explains the inert particle codeposition process, and also describes the plating process as a function of various experimental variables. This model was able to predict the deposit composition and current efficiency.

New plating processes for deposition of Fe-Ni-SiO_2, Zn-Ni-P, Zn-Ni-SiO_2, Zn-Ni-Cd, Zn-Ni-P-Cd and Zn-Ni-P-Mo resulted from the AESF support, which improved the barrier properties of Zn and Zn-Ni alloys. The process parameters and bath constituents for deposition of Zn-Ni-X (X=SiO_2, P, Mo, Cd, Ce) ternary alloys were optimized in order to deposit films with low electronic conductivity and low coefficient of friction. In addition to the sacrificial coating providing protection itself for the underlying metal, the smaller difference in corrosion potential between the substrate and Zn-Ni-Cd, Zn-Ni-P-Cd, Zn-Ni-SiO_2, Zn-Ni-P-Mo and Zn-Ni-Cd-SiO_2 permeation and prevents the hydrogen embrittlement in the substrate. His theoretical studies indicated that the cathodic sites on the protected steel substrate have smaller overpotential than when galvanically coupled with Zn or Zn-Ni alloy.

Galvanostatic pulse and pulse reverse regimes were used to evaluate the kinetics of adsorption/desorption processes or organic compounds and their influence on dissolution and deposition of Fe-Ni, Fe-Ni-SiO_2, Zn-Ni and Zn-Ni-Cd deposited ternary alloys on carbon steel and stainless steel substrates. Mass transfer of the electroactive species within the diffusion layer and the solution equilibrium was found to have a crucial role on the composition of deposited alloys.

A novel one-step electrocatalytic-electroless process was discovered by Dr. Popov at USC for depositing thin nano-structured layers of Ni-P, Co-P, Pd-P and Ni-Co-P composites on metal hydride (MH) particles (powders). Using these processes, high-performance anode materials have been developed for Ni-MH batteries with high capacity, longer cycle life, low self-discharge, uniform operation at high temperatures and corrosion resistance. This process controls the particle size of the alloy and forms protective coating on the surface. Using this process, it is possible to decrease the particle size to a level at which the rate of pulverization dramatically decreases. Because the particles are encapsulated at their optimized size, the corrosion and, consequently, the capacity fade were drastically reduced.

For DOE's Office of Basic Energy Science, a novel Li-ion battery is under development that utilizes a composite anode based on carbon-encapsulated (deposited thin film of Ni-P, Pd-P Sn-P composites.

Dr. Popov's studies carried out at the University of Illinois, the University St. Kiril & Metodij, and his recent work at Texas A&M University and at USC in the area of electrochemical deposition of In, Mo, Zn, Ni, Cr in molten LiC-KCl eutectic at 450°C are of major importance for developing novel cathode materials with superior corrosion performance for molten carbonate fuel cells.

A theoretical model was developed for Sandia National Laboratories for electroless deposition of copper on a planar electrode, and it was used to make time-dependent predictions on the various quantities of the system. Electroless copper was deposited from a tartrate-complexed bath onto a Pd-catalyzed polyimide substrate. The experimental dependence of the thick-ness and quality of electroless copper was determined as a function of the electrolyte pH, HCHO concentration, and copper concentration.

A mathematical model was developed for the characterization of hydrogen permeation into deposited Zn, Bi, ternary and ternary alloys based on Zn-Ni-X (X=P, SiO_2, Mo and Cd, Mo) alloys under corroding conditions.

Currently, Dr. Popov is developing for ONR, NASA, ELISHA Technologies and Sandia National Laboratories novel new treatments for deposition of Fe-Ni, Fe-Ni-SiO_2, Fe-Ni-P, Zn-Ni-X (X=P, SiO_2, Mo, Cd) and Zn-Ni-Cd-based alloys that completely inhibit the hydrogen permeation in the substrate. Development of mathematical models, which will explain the inert particle codeposition and to describe the plating process as a function of various experimental variables, is in progress.

The novel capacitators under construction in the Center for Electrochemical Engineering are based on Dr. Popov's microencapsulations technology of carbons with nanostructured deposits of Ni, Co, Mo or Ru.

As the recipient of the 2002 award, Dr. Popov will present the William Blum Lecture at SUR/FIN 2003 in Milwaukee, Wisconsin.